Threshold Voltage Cancellation For Low Input Voltage of 65nm CMOS Rectifier of Energy Harvesting For Implantable Medical Devices in Telemedicine Embedded System

[1]Hafez Fouad, [2]Hesham Kamel
[1]Micro-electronics Dep, Electronics Research Institute, Cairo, Egypt
[2]Electronics and Communication Dep, Canadian International College, Giza, Egypt

Abstract —
Telemedicine applications run at very low voltages, necessitating the use of a Great Precision Rectifier with high sensitivity to function at low input voltages. In this study, we used a 65 nm CMOS rectifier to achieve a 0.2V input voltage for Energy Harvesting Telemedicine application. The suggested rectifier, which has two-stage structure and operates at frequency of 2.4GHz, has been found to perform better in cases where the minimum operating voltage is lower than previously published papers, and the rectifier can operate over a wide range of low input voltage amplitudes. Full-Wave Fully gate cross-coupled Rectifiers (FWFR) CMOS Rectifier Efficiency at Freq of 2.4 GHz: With an input voltage amplitude of 2V, the minimum and maximum output voltages are 0.49V and 1.997V, respectively, with a peak VCE of 99.85 percent and a peak PCE of 46.86 percent. This enables the suggested rectifier to be used in a variety of vibration energy collecting systems, including electrostatic, electromagnetic, and piezoelectric energy harvesters. The proposed rectifier, which is built at 2.4GHz and has a two-stage structure, performs better in the event of low input voltage amplitude and has a lower minimum operation voltage than previously published papers. Full-wave fully gate cross-coupled rectifiers (FWFR) CMOS Rectifier Performance Summary at Freq of 2.4 GHz: With a 2V input voltage amplitude, the minimum and maximum output voltages are 0.49V and 1.997V, respectively, with a maximum VCE of 99.85% and a maximum PCE of 46.86%.

Keywords__ High Precision Rectifier, Wide-Band Active Rectifier, Energy Harvesting, Embedded system, IoT Telemedicine System, Threshold voltage minimization, Differential drive CMOS rectifier, Full-wave fully gate cross-coupled rectifiers (FWFR).

I. INTRODUCTION

A. Implantable Medical Device IMD Applications

Implantable medical devices, IMD, are increasingly being used to improve the medical outcomes of patients. Therefore, implantable medical devices (IMDs) are typically used to monitor and treat a variety of medical conditions. Today, wireless modules are an important part of many modern IMDs. Therefore, doctors can use the device programmer wirelessly to configure IMD parameters. However, such wireless technologies expose IMD to security attacks. Therefore, security and privacy issues are urgent design issues in telemedicine embedded systems.
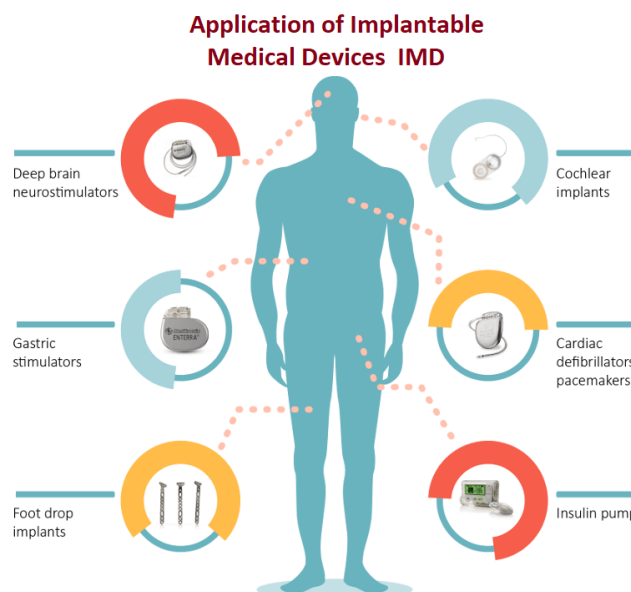

Fig.1.a Implantable Medical Device IMD Application[1]

B. Challenges for Implantable Medical Devices IMDs

IMD designers have already considered safety, reliability, complexity, power consumption, and cost. but, current studies has proven that designers have to additionally don't forget protection and facts privateness to defend sufferers from acts of robbery or malice, in particular as clinical era turns into more and more related to different structures through wi-fi communications or Internet. As developments in energy efficiency, sensing, wi-fi structures and bio-interfaces make viable new and advanced IMDs, additionally they underscore the significance of knowledge and addressing protection and privateness issues in an more and more related global as proven in Fig.2 . Energy harvesting structures has turn out to be the maximum crucial troubles because of the vulnerable sign from the human body.
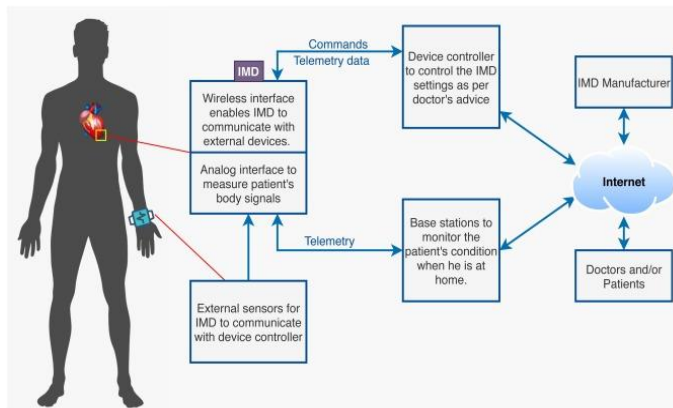

Fig.1.b Telemetry, Security and privacy concerns in IMD

C. Energy Harvesting and Powering of IMD

Due to weak coupling, skin absorption, and a narrow bandwidth passage, wireless power transfer technology has a very low power transfer efficacy. Therefore, it is vital to utilize an effective rectification mechanism to handle the power received from the coupling coil's secondary winding. Telemedicine Embedded systems sometimes receive low voltage levels of vital signs in the human body to diagnose the patient's health. Therefore, it is necessary to design a low threshold voltage rectifier that can detect low input voltage. Which parameter affects the threshold voltage? In Figure.2, the threshold voltage depends on the following parameters: 1. Gate material, 2. Gate insulator, 3. Gate insulation thickness, 4. Channel doping, 5. Impurities on the Silicon Insulator interface, 6. Voltage between source and board, 7. temperature.

An important value that characterizes MOSFET transistors is the threshold voltage value. Depending on the type of MOSFET, the threshold voltage value can be positive or negative. This value can be controlled during the MOSFET transistor manufacturing process. The effects of channel length L, drain (source) region depth xj, consuming-source voltage (VDS) on voltage term ΔVto are shown in Figures 1, 2, and 3 [2].
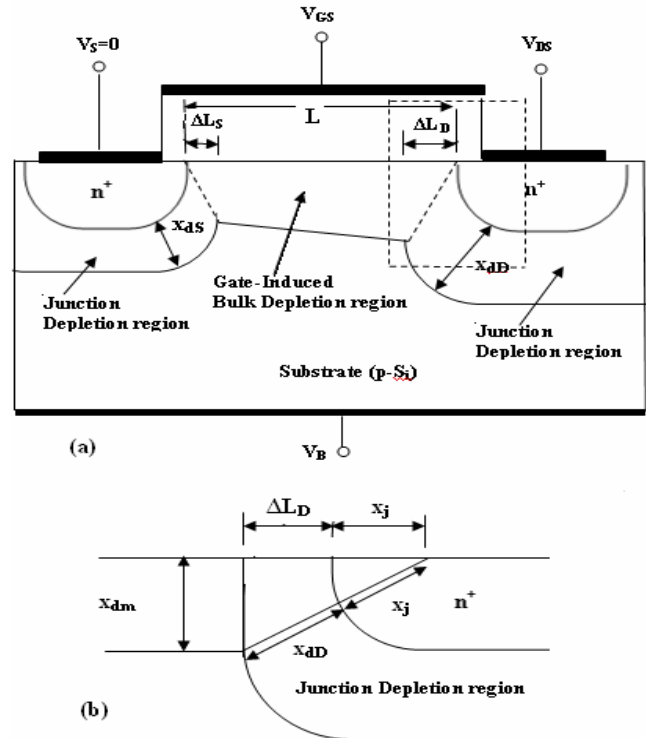

Fig.2a Simplified geometry of MOSFET channel region, with gate-induced bulk depletion region and pn-junction depletion region. (b) Close-up view of drain diffusion edge [1]
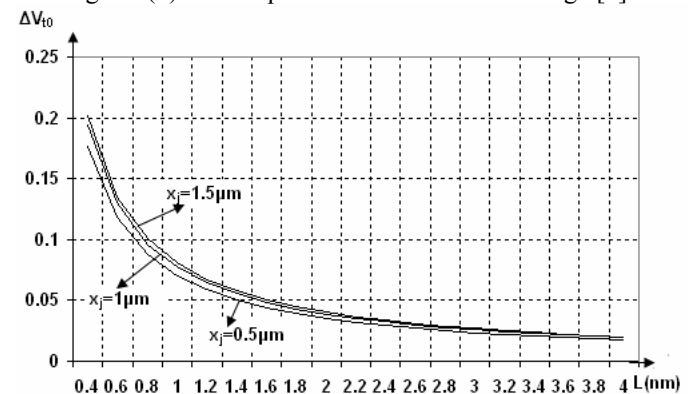

Fig.2c Dependence of ΔVto on length L for parametric values of depth xj, when NA = 1016 cm-3, ND = 1018 cm-3, tox = 20 nm and VDS = 0V[2].

Based on obtained values which might be represented in Fig.1, Fig.2 and Fig.3, for L ≈ xj the ΔVt0 can have an impact on in discount of the edge voltage Vt0. While if L >> xj the ΔVto isn't massive, the NMOS is described as long-channel device. Booming cost of bounds NA and

xj can have small have an impact on in time period of the edge voltage ΔVto. The VDS voltage can have massive have an impact on withinside the time period ΔVto, which ends up in large cost for better cost of VDS [3].
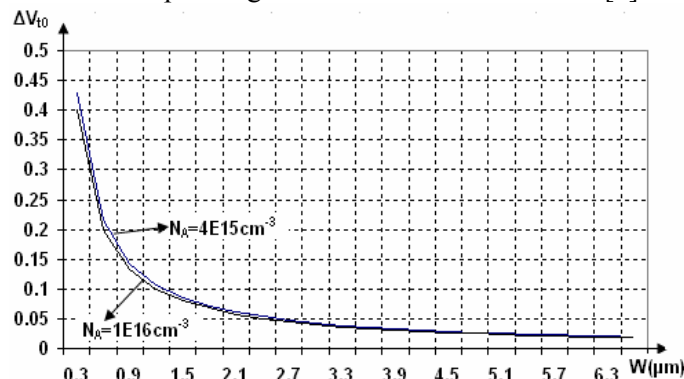

Fig.3 Dependence of ΔVt0 on channel width (W) for parametric values of NA, when ND=1018cm3 and tox=20 nm.

The dependency of the voltage term Vto on the channel width is given in Fig.3, and we can conclude that when W xdm, the Vt term will affect the growth of the total threshold voltage, however when W >> xdm, the Vt term is not important.

D. Calculation of threshold voltage of NMOS with short-channel

If the channel length of a MOSFET transistor is on the order of thickness of source and drain junction depletion region, it is referred to as a short channel device. If the effective channel length Leff is almost equal to the S and D junction depth xj, the MOSFET can be classified as a short channel device (Figure 2). The length of the channel has an influence if IGMP is specified as a short channel device. Threshold voltage is a term that refers to the voltage that a device When compared to long channel devices, short channels drop the threshold voltage from V to [4, 5].

$$Vto \ (short \ channel) = Vto \ - \Delta Vto \qquad (1)$$

Let ΔLS and ΔLD denote the lateral extent of the depletion zones associated with the source and drain junctions, respectively, as shown in Fig 3. The charge within the trapezoidal region's bulk depletion region is then:

$$Q_{Bo} = -\left(1 - \frac{\Delta L_S + \Delta L_D}{2 \cdot L}\right)\sqrt{2qN_A\varepsilon_{Si}| - 2\Phi_F|} \qquad (2)$$

After calculation the ΔL_S and ΔL_D, the amount of threshold voltage reduction ΔVto can be found as [5, 6]:

$-x_{dS}$, x_{dD} represent the depth of depletion regions at source and drain as results of pn junction, respectively.

$$\Delta V_{to} = \frac{1}{C_{ox}}\sqrt{2qN_A\varepsilon_{Si}| - 2\Phi_F|}\ \frac{x_j}{2L}\left[\begin{array}{c}\left(\sqrt{1 + \frac{2x_{ds}}{x_j}} - 1\right)\\ +\left(\sqrt{1 + \frac{2x_{dD}}{x_j}} - 1\right)\end{array}\right] \qquad (2)$$

E. Calculation the threshold voltage of NMOS with narrow-channel

If the channel width of a MOSFET transistor is on the same order of magnitude as the maximum depletion area thickness into the substrate, it is called a narrow-channel device (xdm). When compared to a long-channel device, this effect has an impact on the threshold voltage, resulting in a greater value for Vt0 [7, 8].

$$Vto \ (narrow\text{-}channel) = Vto \ + \Delta Vto \qquad (4)$$

If the geometries of the depletion area edges are described by quarter-circular arcs, the voltage term Vto as a result of narrow-effects is [9]:

$$\Delta V_{to} = \frac{1}{C_{ox}}\sqrt{2qN_A\varepsilon_{Si}| - 2\Phi_F|}\ \frac{\pi \cdot x_{dm}}{2\,W} \qquad (5)$$

After calculating ΔLS and ΔLD, the amount of decrease in threshold voltage ΔVt0 can be calculated as [2, 5]. xdS, xdD signify complexity of the source and drain depletion regions resulting from pn junction. For long channels The device will have a lower threshold voltage if: Substrate doping is reduced (NA), oxide thickness is reduced (tox), oxide interfacial charge is increased (has little effect): Nox) [10]. For short channel devices, the threshold voltage is the Vt term compared to long channel devices, channel length (L), junction depth (xj), drain diffusion doping (small effect), and drain-source. Voltage (VDS).

When compared to long-channel devices, we will enhance the threshold voltage for narrow channel devices by (Vt term), which is dependent on: channel width (W), maximal depletion area thickness (xdm). The positive source-to-substrate voltage VSB causes the rise in total threshold voltage (body effect, as in IC). Finally, for MOSFETs with a restricted channel length and a modest channel width, the threshold voltage variations caused by short- and narrow-channel effects may tend to cancel each other out [11].

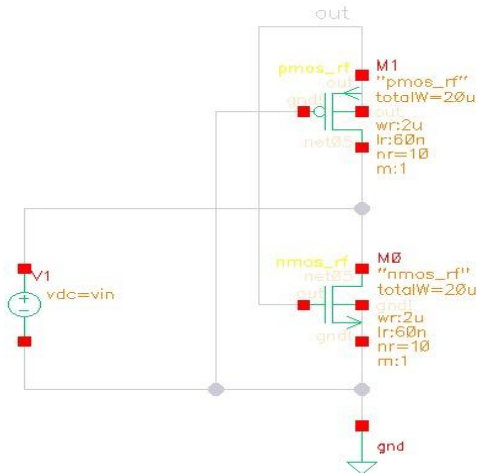Optimize the effective parameter on Vth cancellation

Fig.4 Threshold Voltage cancellation of CMOS Rectifier

Circuit topology, diode device specifications, RF input signal frequency and amplitude, and output load conditions all impact CMOS rectifier voltage conversion efficiency (VCE) and power conversion efficiency (PCE). The ratio of DC output voltage VOUT to input peak voltage amplitude | VAC | is known as VCE and may be written as :

$$VCE \ = \ \frac{Vout}{|VAC|} = \frac{Vout}{Vout + Vdo} \qquad (6)$$

Where Vdo is the total dropout voltage along the rectifier's conduction path. PCE is also defined as the ratio of output power Pout to input power Pin. In fact, the PCE of the rectifier is given as follows:

$$PCE \ = \ \frac{Pout}{|Pin|} = \ \frac{Vout}{|VAC|} \ x \ \frac{Iout}{Iin} \qquad (7)$$

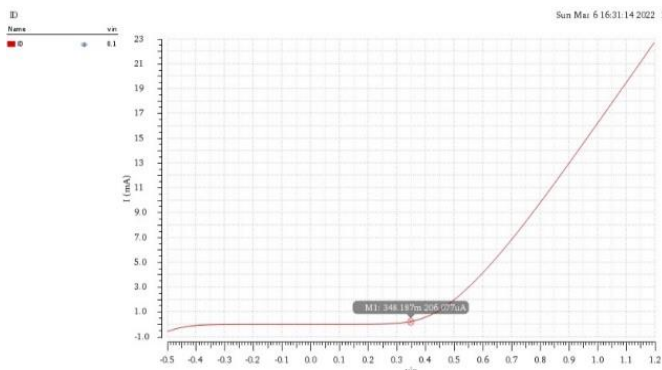Where Iout is the output DC current and Iin is the total input current of the rectifier.

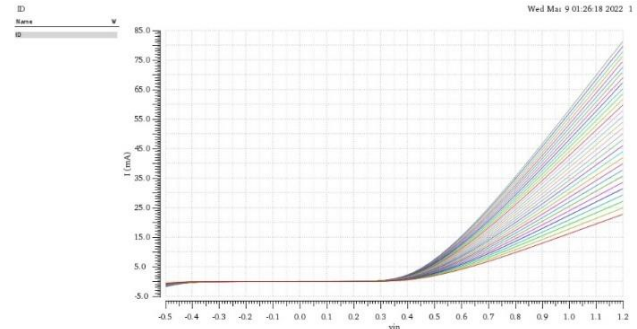Fig.5 optimize the most effect parameter on Vth cancellation

Fig.6. Sweep Analysis of Gate width W with Vth
A slightly change of Vth due to Optimize the Gate width W

II. OPTIMIZATION OF FOUR RECTIFIERS DESIGNS AND SIMULATION RESULTS

As shown in Table.1, the proposed four rectifier circuits were designed using 65nm CMOS technology. We used a cadence tool to perform circuit simulations to optimize performance obtaining the specifications required for proposed design.

The first method cancels MOSFET threshold voltage by applying a gate bias generated from output voltage of rectifier, as shown in Figure 4. This technique provides simple architecture at expense of high reverse current. Upgraded version of the SVC technique is depicted in [8]. 2 Cross-coupled differential CMOS architecture shown in [8] provides better PCE than the SVC scheme. However, the promised VCE will not be provided. An active rectifier architecture based on a 3CMOS inverter is proposed in [9]. It provides good VCE and PCE by reducing both reverse current and threshold voltage. [10,11] uses a technique based on four bootstrap capacitors. Decrease the effective threshold voltage of the main path transistor and increase VCE and PCE.

Table.1 Four Proposed Rectifier Designs

1	Self-VTh Cancellation (SVC) Rectifier	
2	Cross-coupled differential CMOS Rectifier	
3	CMOS Negative Voltage Converter Rectifier	
4	Bootstrapped capacitor-based Rectifier	

The following sections describe in details circuit design parameters and simulation results

A. CMOS Negative Voltage Converter Rectifier

The first stage of rectifier design is called the negative voltage converter and is used to positively convert the negative half cycle of the input sine wave. This is done using two PMOS transistors and two NMOS transistors, as shown in Figure 7. In the input cycle, node

1 is usually at higher latent and node 2 is at lower latent. As a result, the majority of the MIMO transistors can be connected directly to node 1 and the MIMO can be connected to node 2.

In this case, there is no voltage drop Vth. The voltage drop is only *Vdsp + Vdsn* in each conduction leg. Here, *Vdsp and Vdsn* are generated by the on-resistance of the transistor. Therefore, you can minimize the voltage drop by using a large transistor size to reduce resistance and obtain a small voltage drop.
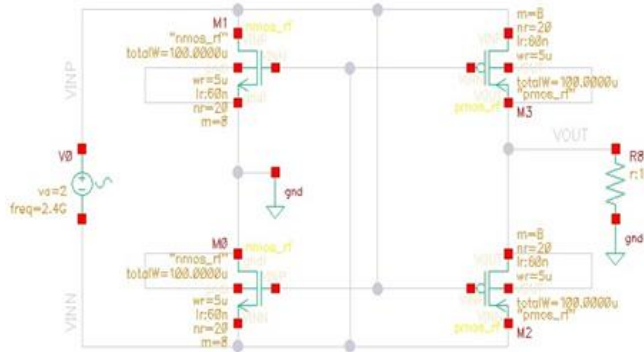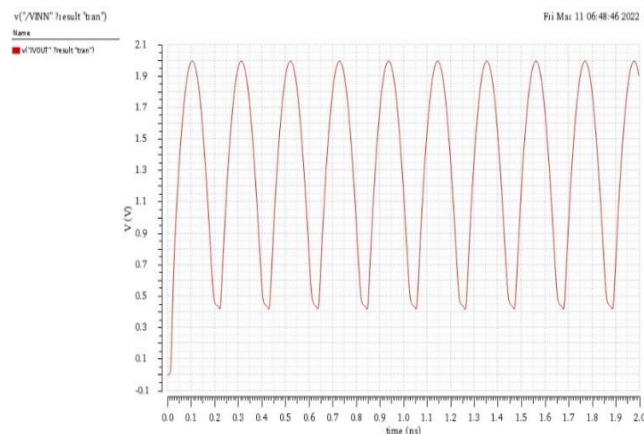

Fig.7a. CMOS Negative Voltage Converter

Fig.7b. Waveform of CMOS Negative Voltage Converter. input voltage minimum was 0.35V

B. Self-VTh Cancellation (SVC) Rectifier Design

In recent years, several VTh suppression strategies have been developed to lower the effective threshold voltage in order to obtain high VCE and PCE. The SVC rectifier is seen in Figure 2, 3 [16,17]. The output terminal and ground terminal of the SVC rectifier are linked to the gates of nMOS and pMOS transistors, respectively. It has a straightforward rectifier design with low input power and high PCE. A static gate-source voltage is provided to the MOS transistor in this design, lowering the effective VTh for high DC bias voltage. In recent years, several VTh suppression strategies have

been developed to lower the effective threshold voltage in order to obtain high VCE and PCE. The SVC rectifier is seen in Figure 1 [12,13]. The output terminal and ground terminal of the SVC rectifier are linked to the gates of nMOS and pMOS transistors, respectively. It has a straightforward rectifier design with low input power and high PCE. A static gate-source voltage is provided to the MOS transistor in this setup, lowering the effective VTh. This architecture increases the reverse leakage current when the DC bias is strong, impacting the VCE and PCE as a whole. The same author presents the improved architecture in [8]. MOSFET threshold voltage is cancelled by applying a gate bias generated from the output voltage of the rectifier. Figure 8a Self-suppressing rectifier (SVC) design. In the SVC waveform in Figure 8b, the input is the blue curve, the red is the output, and the minimum input voltage is excellent, but the maximum is significantly reduced. The minimum input voltage is 0.267V, maximum input voltage being 1.478V.

Because the input signal given by secondary windings of wireless power transfer system is relatively modest, low turn-on voltage is an essential consideration in diode devices. The relatively high threshold voltage of diode-connected MOS devices limits their performance. Using threshold cancellation methods, VCE and PCE may be greatly boosted. Another aspect that affects the performance of MOS-based diodes is reverse leakage. In order to increase overall performance, different threshold and reverse current suppression strategies for MOS-based diodes have been presented in recent years. In [14,15], the Self Vth Cancellation (SVC) approach is presented.
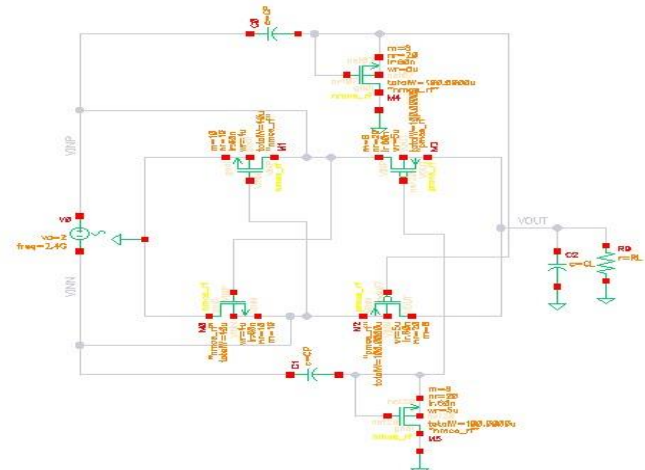

Fig.8a Self-Vth Cancelation (SVC) Rectifier Design

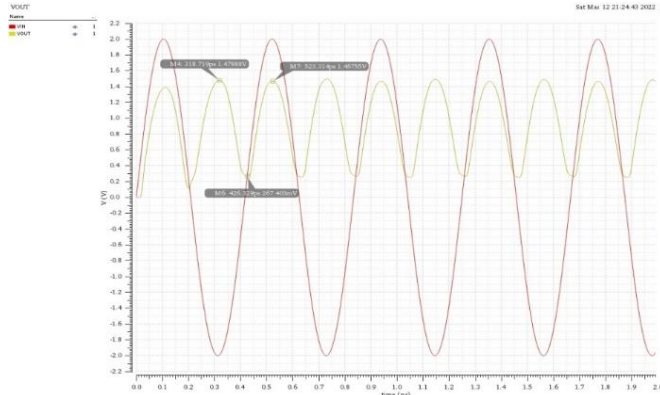Fig.9b Waveforms of Differential drive CMOS rectifier

Fig.8b Waveforms of SVC, The input is the blue curve while red one is the output, the input minimum voltage is better but the maximum is reduced. The min input Volt is 0.267 V while the max input Volt is 1.478 V

C. Differential-drive CMOS Rectifier Architecture

A cross-coupled differential drive CMOS rectifier design is shown in Figure 9. Bridge structure in a cross-coupled differential CMOS system. The differential mode signal actively biases the gate of the MOS transistor in this differential system. With a negative gate bias, this approach efficiently reduces the MOS transistor's on-voltage and rapidly suppresses the reverse leakage current. Although this architecture has a high PCE, it does not have a decent VCE. A decent VCE needs multiple phases, some of which may impose spatial constraints. As a result, this architecture is unsuitable for today's smaller bio-implantable electronics.
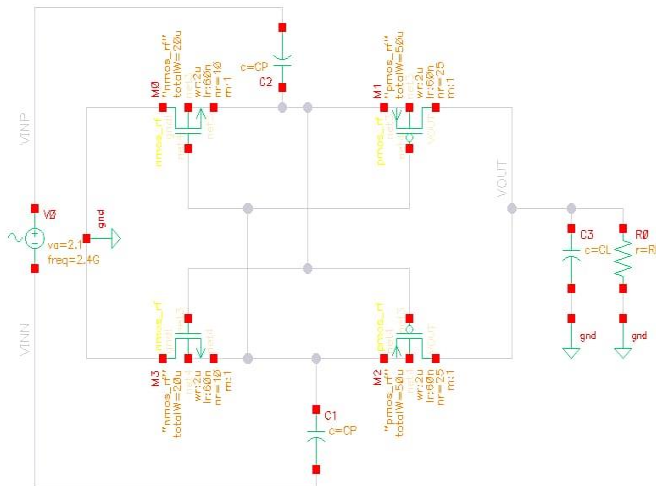
D. Design-3 Bootstrapped capacitor-based rectifier :

To lower the effective threshold voltage, a bootstrap capacitor is employed, and CMOS inverter is used to limit reverse current. High power conversion efficiency (PCE) is achieved at price of low dropout voltage in the planned architecture. The suggested design is well-suited to low-voltage power supply and high-current loads. In a cadence scenario, the suggested rectifier is built in typical 65nm CMOS technology. In comparison to the findings of the best CMOS rectifiers released recently, the simulation demonstrates that the voltage and power conversion efficiency is enhanced in a limited layout physical -area.

In comparison to [18,19] and 0.28 from 0.5V to 1V, the minimum working voltage is lower, and the rectifier has LIV (low input) with a broad range of input voltage amplitudes from 0.1V to 2.2V. It can operate with voltage). V to 0.7V at [20, 21]. This enables the rectifier to function with a variety of energy collecting systems, including vibration energy harvest, electrostatic energy harvest, electromagnetic energy harvest, and piezoelectric energy harvest.

Voltage efficiency Yv is defined as the proportion of the output DC voltage Vout and the input voltage amplitude |Vin|, as shown in Eq (8). With larger load resistors, the rectifier's output voltage efficiency improves due to its high output voltage drop. [22, 23]

$$\mathfrak{y}_v = Vout \, / \, |Vin| = 100\% \qquad (8)$$

Power Efficiency of Rectifier is calculated as:

Fig.9a Design 2 - Differential drive CMOS rectifier

$$\mathfrak{y}_P = \frac{\int_{t_1}^{t_1+T} v_{out}(t) \cdot i_{out}(t)\, dt}{\int_{t_1}^{t_1+T} v_{in}(t) \cdot i_{in}(t)\, dt} \qquad 100\% \qquad (9)$$

Where T is the duration of the input signal and t1 is the start time. The efficiency drops as RLoad increases because the current through ohmic load decreases and tends to the current through the comparator. The load capacitor, which is tuned for the applied frequency, has a capacitance of 10uF and a load of 50K.
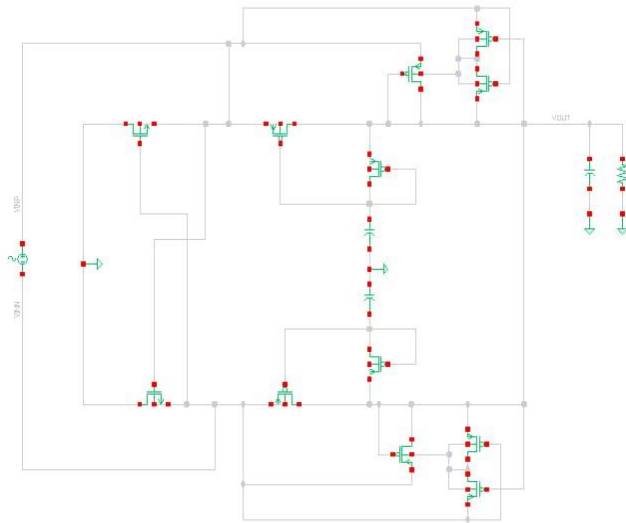

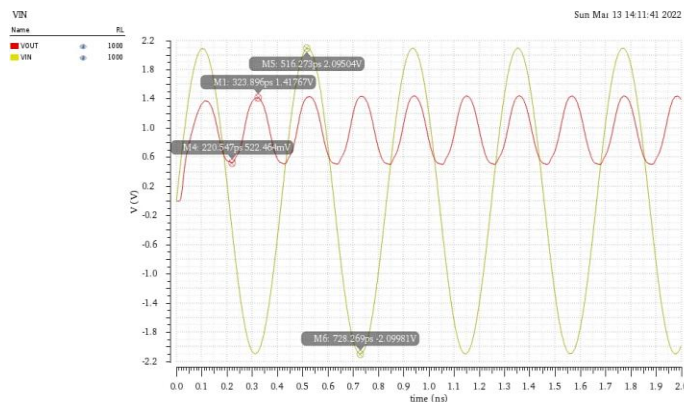Fig.10.a Design-3 Bootstrapped Capacitor-based Rectifier

Fig.10.b Waveforms of Bootstrapped capacitor-based rectifier

III. PROPOSED DESIGN OF CMOS RECTIFIERS

This section will involve the schematic, the detailed explanation and layout of two proposed CMOS rectifiers using 65 nm CMOS technology.

A. Differential drive CMOS rectifier with external bootstrapping circuit

A.1 Description:

The suggested full-wave differential drive rectifier method is depicted in Figure 11. The transistor M2, wired as a nMOS diode, conducts during positive half cycle of the differential input voltage Vin and supplies the current

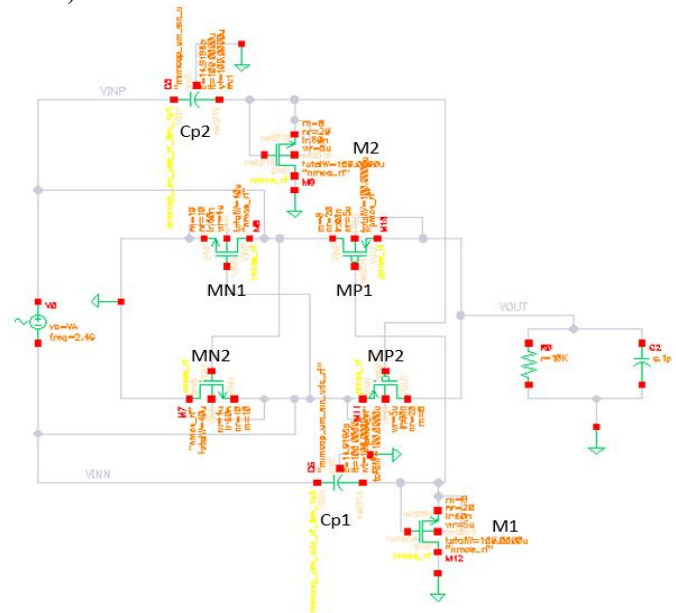needed to charge the bootstrap capacitor Cp2 (Vina-Vthn).

Fig.11: Differential drive CMOS rectifier schematic with external bootstrapping circuit

In the conduction phase, the pMOS switch Mp2 is driven by the sum of the single-ended input voltage Vina and the Cp2 capacitor voltage. The same procedure is used for the pMOS switch Mp1. The gate bias of the pMOS transistors (Mp1, Mp2) becomes more negative than in conventional mode, and the rectifier begins at a lower input voltage. To meet the dynamic threshold compensation method, the body terminals of all transistors are linked to increase their threshold voltages during the off state and decrease them during the onstate.

Fig.11 shows the schematic of the rectifier working at center frequency of 2.4 GHz. The transistor sizes of the NMOS are 400 μm but the bootstrapping transistors are 800 μm same as the PMOS transistors, bootstrapping capacitors are 15 pF. All transistors use the minimum length 60 nm.

Advantages:
- Because the gate bias voltages of pMOS transistors (Mp1, Mp2) become more negative than in the typical mode, the rectifier starts up with a lower input voltage.

Disadvantages:
- Large area due to the usage of capacitors and two diode connected transistors in addition to the 4 transistors used in rectifying the signal.
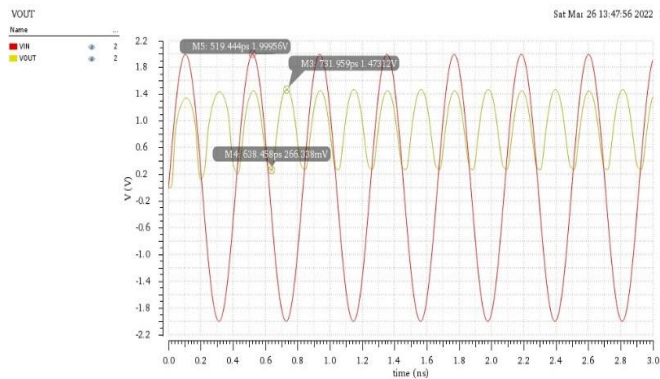
A.2 Simulated Results

Fig.12: Input and output waveforms at F = 2.4 GHz

A.3 Performance Summary of Differential drive CMOS Rectifier with external Bootstrapping circuit - at Freq of 2.4 GHz

With an input voltage amplitude of 2V, the lowest and highest output voltages are 0.265V and 1.467V, correspondingly., peak VCE ($\frac{V_{out}}{V_{in}}$) = 93.9 % and peak PCE ($\frac{P_{out}}{P_{in}}$) = 15.8 %.
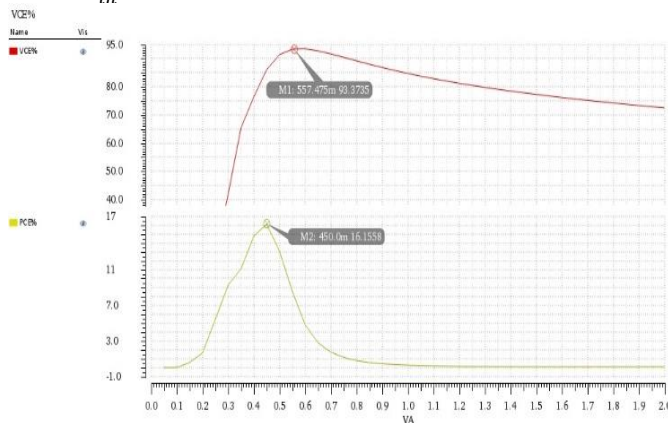

Fig.13: VCE and PCE at F = 2.4 GHz

A.4 Layout of the Differential drive CMOS rectifier with external bootstrapping circuit

Figure 14 shows the layout of Differential drive CMOS rectifier with external Bootstrapping circuit. The area of the layout is 0.183 mm x 0.324 mm = 0.059 mm^2. The layout is built using Cadence tools.
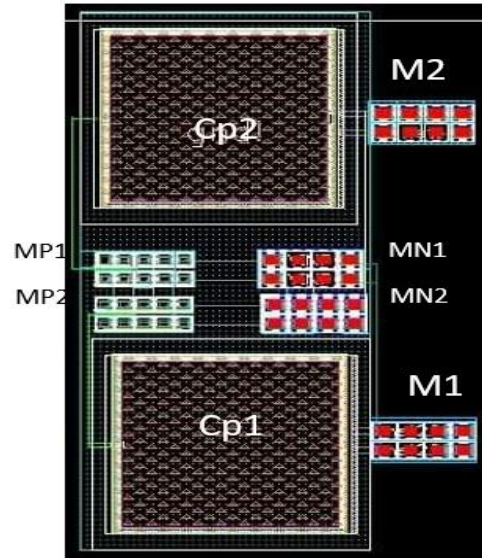

Fig.14: Differential drive CMOS rectifier layout with external Bootstrapping circuit

B. Full-Wave Fully gate cross-coupled Rectifiers (FWFR)

B.1 Description:

Here transistors act as switches in the positive half cycle M1, M2 transistors are ON and M0, M3 are OFF in the negative half cycle M0, M3 transistors are ON and M1, M2 transistors are OFF. The FWFR proposed design will be given in this section. Fig.15 shows the schematic of the rectifier working at a center frequency of 2.4GHz. The transistor sizes of the NMOS and PMOS are 960 μm and all transistors use the minimum length 60 nm.

Advantages:
- This circuit addresses the issue of diode-tied MOS transistor threshold voltage drop.

Disadvantages:
- The flow-back current from the storage capacitor to the antenna, as well as other parasitic currents, reduce the power efficiency of this device.
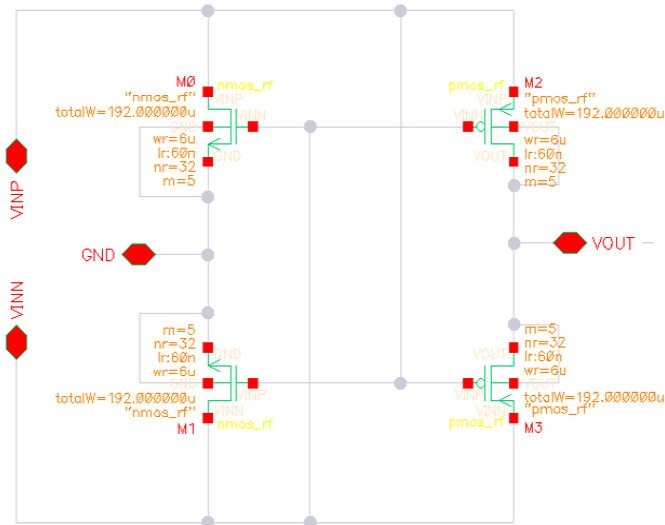
Fig.15: Schematic View of FWFR CMOS Rectifier

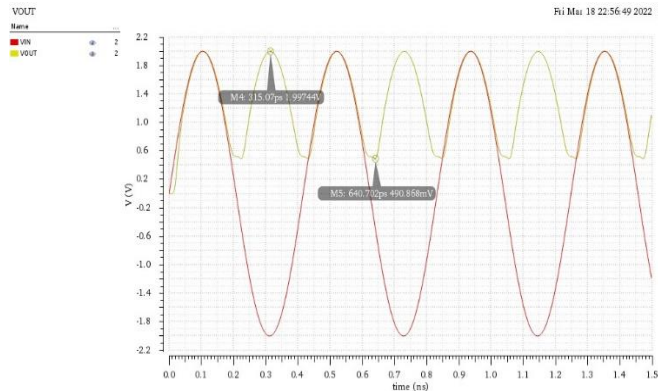## B.2 Simulated Results

Fig.16: Input and output waveforms at F = 2.4 GHz
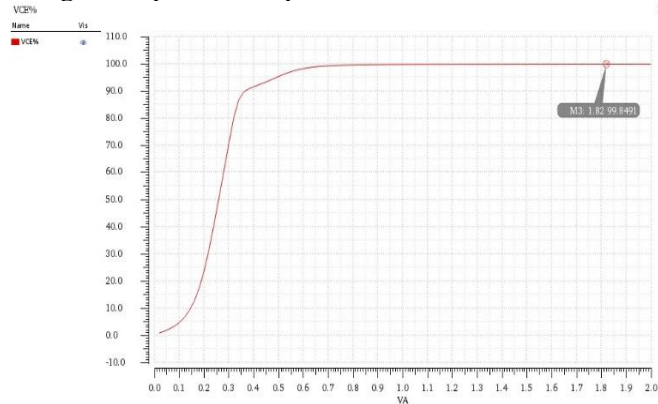
Fig.17: VCE at F = 2.4 GHz

B.3 Performance Summary of FWFR CMOS Rectifier at Freq of 2.4 GHz

The minimum and maximum output voltages generated using input voltage amplitude of 2V are 0.49V and 1.997V respectively, maximum VCE ($\frac{V_{out}}{V_{in}}$) = 99.85 %

and maximum PCE ($\frac{P_{out}}{P_{in}}$) = 46.86 %.

Fig.18: PCE at F = 2.4 GHz

B.4 Layout of the FWFR CMOS Rectifier

Fig.19: Layout of the FWFR CMOS Rectifier

Fig.19 shows the layout of second proposed CMOS Rectifier, taking into consideration the widths of the wires. The area of layout is 0.117mm x 0.079mm = 0.009mm2. The layout is built using Cadence.

Fig.20 EM simulations for wires connection

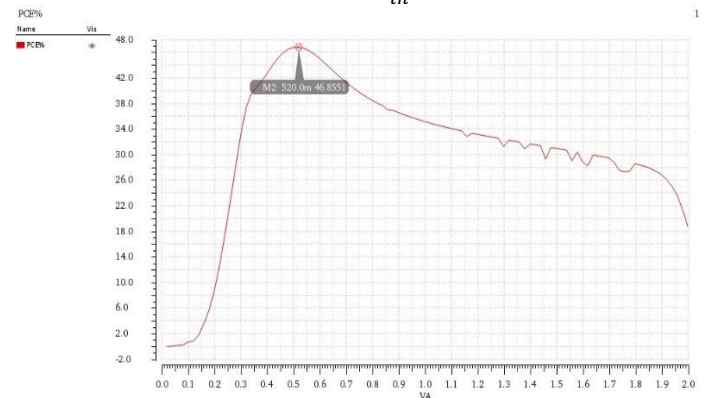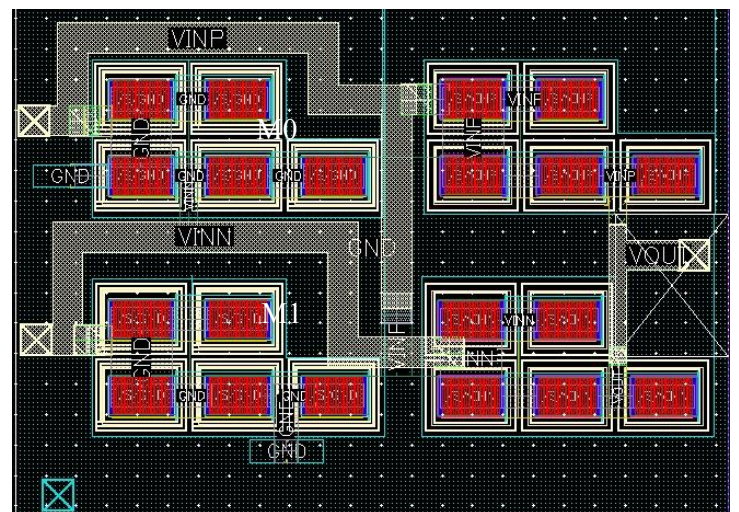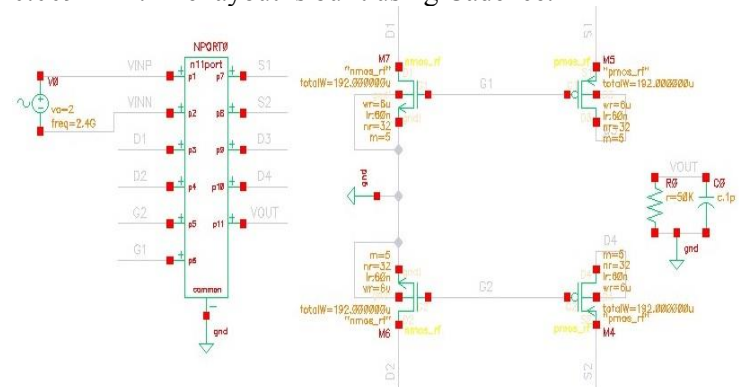Figure.20 show the EM simulations for all the wires connecting between the 4 transistors and made the required sp file
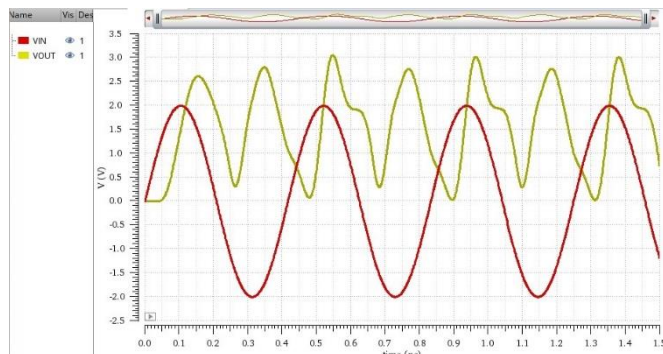

Fig. 21 The red curve is the differential input and the yellow one is the output one

IV. PERFORMANCE COMPARISONS

In this section we compare our proposed designs among themself and compare the best two designs compared to the previous research. In order to be able to rank the designs, we identified the most important factors PCE and VCE and follow ranking methodology described in Fig.20. According to flow chart in Fig.20, the selection criteria was done by giving score for both PCE and VCE and calculate weighted average score as follows:

PCE Score (%) = PCE %/ PCE % best score   (a)
VCE Score (%) = VCE % / VCE % best score   (b)
Overall Score Average Score = 50% * PCE Score (%) + 50% * VCE (Score %)   (c)

Fig.22 Ranking methodology of Rectifier Designs

Table.2. provide detailed of all results and Design Performance assessment based on our proposed assessment methodology in Fig.20. According to Table.2. we selected the top two options and perform detailed layout using Cadence Layout module. The model show that first rank is cross coupled FWFR CMOS rectifier topology and second is differential drive rectifier topology . As final conclusion we found the first rank has net area XX mm2 and second rank has xx mm2 so by selecting the minimum layout area the best option will b e YY model

Table.2 All Results of Proposed Designs and Assessment

Parameters	First Design	Second design	Third Design	Fourth Design
Rectifier Topology	Cross Coupled	Differential Drive	Bootstrapped Capacitor	Vth-Cancellation
Vout DC	419.68mV - 1.464 V	522.46 mV - 1.4176 V	265.515 mV - 1.467 V	490.868 mV - 1.997 V
PCE %	30.55%	13.85%	15.787%	46.855%
VCR % S	94.4%	64.19%	93.91%	99.849%
Score Output Range	69.3%	59.4%	79.8%	100%
Score PCE%	65.2%	29.6%	33.7%	100%
Score VCE%	94.5%	64.3%	94.1%	100%
Score Average	76.3%	51.1%	69.2%	100%
Score Overall	**Second**	**Fourth**	**Third**	**First**

Table.3 Performance Parameters Comparisons between Low Voltage Rectifiers

Performance Parameters	IEICE 2012 [15]	IEEE TCAS I 2011 [16]	**Differental tail drive Rectifier**	**Cross Couple FWFR CMOS**
Technology	0.18um CMOS	0.18um CMOS	65nm CMOS	65nm CMOS
Input Voltage Amplitude	0.28V-0.7V	0.5V-1V	0.21V – 1.95V	0.2V – 1.45V
Working Frequency	10Hz-3KHz	10Hz-10KHz	2.4GHz	2.4GHz
|Vmin|	0.28V	0.5V	0.21V	0.2V
Voltage Efficiency	76%-97% (R_{Load}=40k)	90% (R_{Load}=50k)	94.5 %	71%-81% (R_{Load}=50k)
Power Efficiency	78%-95%	Up to 95%	94.5%	73% -79%

Table.3 compares the performance of this study to that of other rectifiers previously published. Previous rectifiers' lowest functioning voltage was 0.5V in [17] with a 0.5V

low threshold voltage 0.35um CMOS technology. When the input voltage is more than 1V, however, it will not operate, and the application field will be blocked. These flows are addressed by the rectifier suggested in this work. It can not only work with a 0.45V input voltage, but also with input voltage amplitudes ranging from 0.45V to 1.95V, as opposed to 0.5V to 1V in [24] and 0.28V to 0.7V in [25, 26].

In this study, an energy harvesting system with a wide range input voltage amplitude and a highly efficient rectifier is suggested. Under the 65nm CMOS process, the rectifier is ideally suited for input amplitude as low as 0.2V and can function at a wide range of input voltage amplitudes from 0.2V to 2.1V. The suggested rectifier has a maximum voltage conversion efficiency of more than 81% percent and a power efficiency of more than 79% percent. The rectifier's simulated power usage is 0.23 uW at 0.45V, which is approximately 28% less than that of the finest recently reported findings.

V. CONCLUSIONS

The proposed rectifiers are designed for 2.4GHz using a two-stage assembly and an enhanced accuracy active diode in a standard 65nm CMOS process. The lowermost operating voltage is less than in the earlier study, and the rectifier can operate with input voltage amplitudes ranging from 0.2V to 1.95V. This enables the suggested rectifier to be used in a variety of vibration energy collecting systems, including electrostatic, electromagnetic, and piezoelectric energy harvesters. The suggested rectifiers have a highest voltage conversion efficiency of over 81% and a power efficiency of over 79%. The rectifier's simulated power consumption at 0.45V is 0.23 uW, which is roughly 28% less than the best recently reported findings. Mechanical vibrations are the most common energy source accessible in many contexts, which is a benefit of employing them to capture energy.

The proposed rectifier, which is built at 2.4GHz and has a two-stage structure, performs better in the event of low input voltage amplitude and has a lower minimum operation voltage than previously published papers. Full-wave fully gate cross-coupled rectifiers (FWFR) CMOS Rectifier Performance Summary at Freq of 2.4 GHz: With a 2V input voltage amplitude, the minimum and maximum output voltages are 0.49V and 1.997V, respectively, with a maximum VCE of 99.85 percent and a maximum PCE of 46.86 percent. At Freq of 2.4GHz, the performance of a differential drive CMOS rectifier with an external bootstrapping circuit rectifier is

summarised as follows: With a 2V input voltage amplitude, the minimum and highest output voltages are 0.265V and 1.467 V, respectively, with a maximum VCE of 93.9 percent and a maximum PCE of 15.8 percent.

REFERENCES

[1] J. M. Gilbert and F. Balouchi. Comparison of energy harvesting systems for wireless sensor networks. International Journal of Automation and Computing, 5, N. 4:334–347, October **2018**.
[2] V. Raghunathan, A. Kansal, J. Hsu, J. Friedman, and M. B. Srivastava, " Design considerations for solar energy harvesting wireless embedded systems," in Proc. IPSN, Apr. 25–27, **2015**, pp. 457–462.
[3] G. K. Ottman, H. F. Hofmann, A. C. Bhatt, and G. A. Lesieutre, "Adaptive piezoelectric energy harvesting circuit for wireless remote power supply," IEEE Trans. Power Electron., vol. 17, no. 5, pp. 669–676, Sep.**2012**.
[4] Muhammed Emin Başak, Firat Kaçar "A New Fully Integrated High Frequency Full Wave Rectifier Realization" Journal of Microelectronics, Electronic Components and Materials Vol. 45, No.2 **2015**, 101-109, http://www.midem-drustvo.si/Journal%20papers/MIDEM_45(2015)2p101.pdf
[5] C. Sauer, M. Stanac´evic´, G. Cauwenberghs, and N. Thakor, " Power harvesting and telemetry in CMOS for implanted devices," IEEE Trans. Circuits Syst. I, Reg. Papers, vol. 52, no. 12, pp. 2605–2613, Dec. **2015**.
[6] P. Li and R. Bashirullah, "A wireless power interface for rechargeable battery operated medical implants," IEEE Trans. Circuits-Syst.II, Exp.Briefs, Vol.54, no.10, pp.912–916, Oct.**2017**
[7] Hafez Fouad , Hesham Kamel " A Proposed end to end Telemedicine System based on embedded system and mobile application using CMOS Wearable Sensors ", The 2021 International Telecommunications Conference, ITC-Egypt-2021 July 13 - 15, 2021, Air Defence Collage - ADC , Egypt , supported by IEEE , inclusion by IEEE Xplore, SCOPUS
[8] Cevik, I., Huang, X., Yu, H., Yan, M., & Ay, S. U. An ultra-low power CMOS image sensor with on-chip energy harvesting and power management capability. Sensors, 15(3), **2015**, p5531
[9] B. C. Yen and J. H. Lang, "A variable-capacitance vibration-to-electric energy harvester," IEEE Trans. Circuits Syst. I, Reg. Papers, vol. 53, no. 2, pp. 288–295, Feb. 2006. DOI:10.1109/TCSI.2005.856043; Corpus ID: 13862951
[10] Guo, S.; Lee, H. An efficiency-enhanced CMOS rectifier with unbalanced-bias comparators for transcutaneous power high-current implants. IEEE J. Solid State Circuits 2009, 44, 1796–1804.
[11] Din, A.U.; Chung, D.; Park, D.; Lee, H.; Lee, J.-W. A high extraction self-controllable CMOS resonant rectifier circuit for piezoelectric energy scavenging system. In Proceedings of the 2014 International SoC Design Conference (ISOCC), Jeju, Korea, 3–6 November **2014**; pp. 40–41.

[12] Lu, C.; Tsui, C.Y.; Ki, W.H. Vibration energy scavenging system with maximum power tracking for micropower applications. IEEE Trans. Very Large Scale Integr. (VLSI) Syst. 2011, 19, 2109–2119.

[13] Lu, C.; Tsui, C.Y.; Ki, W.H. Vibration energy scavenging and management for ultra low power applications. In Proceedings of the ACM/IEEE International Symposium on Low Power Electronics and Design (ISLPED), Portland, OR, USA, 27–29 August **2017**; pp. 316–321.

[14] Do, X.-D.; Nguyen, H.H.; Han, S.K.; Lee, S.-G. A rectifier for piezoelectric energy harvesting system with series synchronized switch harvesting inductor. In Proceedings of the 2013 IEEE Asian Solid-State Circuits Conference (A-SSCC), Singapore, 11–13 November **2013**; pp. 10–13.

[15] Kwon, D.; Rincón-Mora, G.A.F. A single-inductor 0.35 m CMOS energy-investing piezoelectric harvester. IEEE J. Solid State Circuits **2014**, 49, 2277–2291.

[16] Hafez Fouad, and Hesham Kamel. " Home Rehabilitation of Patient using Bioelectronics Nano-Medicine Devices and 65nm CMOS Embedded Electronics For Insulation To avoid Coronavirus Infection" SSRG International Journal of Electronics and Communication Engineering, vol. 9, no. 4, Apr. 2022, pp. 1-9. Crossref,

[17] Cook BW, Lanzisera S, Pister KSJ. SoC issues for RF smart dust. Proc IEEE 2006;94:1177–96.

[18] Mitcheson PD, Yeatman EM, Rao GK, Holmes AS, Green TC. Energy harvesting from human and machine motion for wireless electronic devices. Proc IEEE 2008;96:1457–86.

[19] Hafez Fouad " A Highly Efficient 0.18um CMOS Rectifier For Vibrational Energy Harvesting System in Embedded Electronics Design", International Journal of Electrical and Electronics Engineering (SSRG-IJEEE), E-ISSN: 2348-8379, P-ISSN:2349-9176, June 2020 Edition ,

[20] Hafez Fouad, Hesham Kamel, Adel Youssef, " Voltage-Booster For CMOS Wide-Band High-Precision Rectifier of Energy Harvesting For Implantable Medical Devices in Internet of Bodies (IOB) Telemedicine Embedded System" SSRG International Journal of Electrical and Electronics Engineering, vol. 9, no. 5, May. 2022, pp. 1-9.

[21] Zhao, T.; Fu, Y.; He, H.; Dong, C.; Zhang, L.; Zeng, H.; Xing, L.; Xue, X. Self-powered gustation electronic skin for mimicking taste buds based on piezoelectric–enzymatic reaction coupling process. Nanotechnology **2018**, 29, 075501.

[22] Jin, W.; Wang, Z.; Huang, H.; Hu, X.; He, Y.; Li, M.; Li, L.; Gao, Y.; Hu, Y.; Gu, H. High-performance piezoelectric energy harvesting of vertically aligned Pb(Zr,Ti)O3 nanorod arrays. RSC Adv. **2018**, 8, 7422–7427.

[23] Qiang Li, Renyuan Zhang, Zhangcai Huang, and Y. Inoue, " A low Voltage CMOS rectifier for wirelessly powered devices," IEEE international Symposium on Circuits and Systems, pp.873-876, May 2010.

[24] C.Peters, J. Handwerker, D. Maurath, Y. Manoli, " A Sub-500 mV Highly Efficient Active Rectifier for Energy Harvesting Applications," IEEE Trans. Circuits Syst. I, Reg. Papers, vol. 58, no. 7, pp. 1542- 1550, July. 2011.

[25] Dan Niu, Zhangcai Huang, Minglv Jiang, Yasuaki Inoue, "A Sub-0.3V highly efficient CMOS rectifier for energy harvesting applications," IEICE NOLTA, vol. 3, no. 3, pp. 405-416, **July 2012**.

[26] Hafez Fouad , " Performance Optimization of Energy Harvesting Solutions for CMOS Circuits in Embedded Electronics Design ", Cogent Engineering, Electrical & Electronic Engineering , Taylor & Francis Group, UK, Vol. 7 , Issue 1 , June 2020, ISSN: 2331-1916,
https://doi.org/10.1080/23311916.2020.1772947
https://www.cogentoa.com/collection/cogent-engineering-best-paper-awards-2017-and-2018